

# Segmentation of Dynamic PET Images Using Cluster Analysis

Koon-Pong Wong<sup>1,2</sup>, Dagan Feng<sup>1,3</sup>, Steven R. Meikle<sup>2</sup>, and Michael J. Fulham<sup>2,4</sup>

<sup>1</sup>Basser Department of Computer Science, The University of Sydney, NSW 2006, Australia

<sup>2</sup>Department of PET and Nuclear Medicine, Royal Prince Alfred Hospital, Camperdown, NSW 2050, Australia

<sup>3</sup>Department of Electronic and Information Engineering, The Hong Kong Polytechnic University, Hong Kong

<sup>4</sup>Faculty of Medicine, The University of Sydney, NSW 2006, Australia

## Abstract

Quantitative PET studies can provide *in-vivo* measurements of dynamic physiological and biochemical processes in humans. A limitation of PET is its inability to provide precise anatomic localisation due to relatively poor spatial resolution when compared to MR imaging. Manual placement of regions of interest (ROIs) is commonly used in the clinical and research settings in analysis of PET datasets. However, this approach is operator dependent and time-consuming. Semi- or fully-automated ROI delineation (or segmentation) methods offer advantages by reducing operator error and subjectivity and thereby improving reproducibility. In this work, we describe an approach to automatically segment dynamic PET images using cluster analysis, and we validate our approach with a simulated phantom study and assess its performance in segmentation of dynamic lung data. Our preliminary results suggest that cluster analysis can be used to automatically segment tissues in dynamic PET studies and has the potential to replace manual ROI delineation.

## I. INTRODUCTION

Nuclear medicine imaging modalities such as PET and SPECT, are able to measure functional changes in local tissues by analysing the underlying tissue time-activity curves (TACs) that are extracted after the manual placement of regions of interest (ROIs) in particular sites of activity. The process of tissue TAC extraction is referred to as ROI analysis. This approach is widely used in clinical and research settings, but it is operator dependent, time-consuming and may not be reproducible. To reduce such subjectivity, semi- or fully-automated methods for ROI delineation (or segmentation) are desirable.

However, automatic segmentation for three-dimensional data is not a trivial task. A number of methods for segmentation of MR datasets have been reported in the literature [1–3]. In MR imaging, it is relatively easy to identify, in the brain, grey matter, white matter, CSF, and extracranial tissues. But segmentation in PET and SPECT is more difficult because in addition to inherent poorer spatial resolution, there is statistical noise due to scatter, signal attenuation and patient motion during scanning.

Multivariate data analysis techniques have been applied in PET and SPECT studies. Principal component analysis (PCA) is perhaps the most frequent approach [4, 5]. PCA explains the variance-covariance structure in multivariate data by linearly transforming

the original set of variables into a smaller set of uncorrelated (orthogonal) variables. In this scheme, the higher order components are important as they explain the major variation in the data, while lower order components are unimportant as they mainly contain noise. Since the lower order components are unimportant, they are discarded without causing significant loss of information. Thus, dimensionality reduction (or data compression) can be achieved using the PCA technique. Factor analysis (FA) can be thought of as a generalisation of PCA as it produces factors closer to the true underlying tissue TACs. It has been used to extract the time course of blood activity in the left ventricle of the heart from PET images [6] and to analyse myocardial perfusion in PET studies [7]. FA segments the dynamic sequence of images into a number of structures which can be represented by functions. Each function represents one of the possible underlying physiological kinetics in the sequence of images. The whole sequence of images can then be represented by a weighted sum of functions. The first step of FA involves performing PCA on the sequence of images. Mathematical transformations such as positivity constraints and rotation of the factors are then performed so that the functions convey physiological meanings.

Cluster analysis is another multivariate approach and it has been used in psychiatry and sociology for many years. One of the major aims of cluster analysis is to partition a large number of objects according to certain criteria into a smaller number of clusters that are mutually exclusive and exhaustive such that the objects within a cluster are similar to each other while objects in different clusters are dissimilar [8]. Cluster analysis has potential value in classifying PET data, because the cluster centroids are derived from many objects (tissue TACs) and an improved signal-to-noise ratio can be achieved [9]. Apparent advantages are the fast generation of parametric images and reduction in storage space. In this work, we describe an approach to automatically segment dynamic PET images using cluster analysis, and we validate it using a simulated dynamic 2-<sup>[11C]</sup>thymidine PET study with a slice of the Zubal phantom [10] and assess it with a dynamic lung [<sup>18F</sup>]fluorodeoxyglucose (FDG) PET study.

## II. MATERIALS AND METHODS

### A. Segmentation Scheme

The segmentation method is based on cluster analysis. Our aim is to classify a number of tissue TACs according

to their shape and magnitude into a smaller number of distinct characteristic classes that are mutually exclusive so that the tissue TACs within a cluster are similar to one another but are dissimilar to those drawn from other clusters. The clusters (or clustered ROIs) represent the locations in the images where the tissue TACs have similar kinetics. The kinetics associated with a cluster (i.e. cluster centroid) is the average of TACs in the cluster. Suppose that there exists  $k$  characteristic curves in the dynamic PET data matrix,  $\mathbf{M}$ , which has  $m$  tissue TACs and  $n$  time frames with  $k \ll m$  and that any tissue TAC belongs to only one of the  $k$  curves. The clustering algorithm then segments the dynamic PET data into  $k$  curves automatically based on a weighted least-squares distance measure,  $\mathcal{D}$ , which is defined as

$$\mathcal{D} \{z_i, \mu_j\} = \sum_{j=1}^k \sum_{i=1}^m \|z_i - \mu_j\|_{\mathbf{W}}^2 \quad (1)$$

where  $z_i \in \mathbb{R}^n$  is the  $i$ -th tissue TAC in the data;  $\mu_j \in \mathbb{R}^n$  is the centroid of cluster  $C_j$ ; and  $\mathbf{W} \in \mathbb{R}^{n \times n}$  is a square matrix containing the weighting factors on the diagonal and zero for the off-diagonal entries. The weighting factors in  $\mathbf{W}$  were chosen to be proportional to the scanning intervals of the experiment.

There is no explicit assumption on the structure of data and the clustering process proceeds automatically in an unsupervised manner. The minimal assumption for the clustering algorithm is that the dynamic PET data can be represented by a finite number of kinetics. As the number of clusters,  $k$ , for a given data set is usually not known *a priori*,  $k$  is usually determined by trial and error [8]. In addition, the initial cluster centroid in each cluster is initialised randomly to ensure that all clusters are non-empty. Each tissue TAC is then allocated to its nearest cluster centroid according to the following criterion:

$$\begin{aligned} \|z_l - \mu_i\|_{\mathbf{W}}^2 &< \|z_l - \mu_j\|_{\mathbf{W}}^2 \\ \Rightarrow z_l &\in C_i \quad \forall i, j = 1, 2, \dots, k, \quad i \neq j \end{aligned} \quad (2)$$

where  $z_l \in \mathbb{R}^n$  is the  $l$ -th tissue TAC in  $\mathbf{M}$ ;  $\mu_i \in \mathbb{R}^n$  and  $\mu_j \in \mathbb{R}^n$  are the  $i$ -th and  $j$ -th cluster centroid, respectively; and  $C_i$  represents the  $i$ -th cluster set. The centroids in the clusters are updated based on equation (2) so that (1) is minimised. The above allocation and updating processes are repeated for all tissue TACs until there is no reduction in moving a tissue TAC from one cluster to another. On convergence, the cluster centroids are mapped back to the original data space for all voxels. An improved signal-to-noise ratio can be achieved because each voxel in the mapped data space is represented by one of the cluster centroids each of which possesses a higher statistical significance than an individual TAC. The algorithm is similar to the  $k$ -means type Euclidean clustering algorithm [11]. However, this latter algorithm requires that the data are normalised and it does not guarantee that the within-cluster cost (and thus the total cost) is minimised since no testing is performed to check whether there is any cost reduction if an object is moved from one cluster to another.

## B. Phantom Study

To examine the validity of the segmentation scheme, we simulated a dynamic 2- $^{11}\text{C}$ thymidine (a marker for cell proliferation) PET study [12]. Typical 2- $^{11}\text{C}$ thymidine kinetics for different tissues were derived from 8 patients. The data were acquired on an ECAT 931 scanner (CTI/Siemens, Knoxville, TN). The dynamic PET data were acquired over 60 min with a typical sampling schedule ( $10 \times 30$  sec,  $5 \times 60$  sec,  $5 \times 120$  sec,  $5 \times 180$  sec,  $5 \times 300$  sec) and the tracer TAC in blood was measured with a radial artery catheter following tracer administration. Images were reconstructed using filtered back-projection (FBP) with a Hann filter cut-off at the Nyquist frequency. ROIs were drawn over the PET images to obtain tissue TACs in bone, bone marrow, blood pool, liver, skeletal muscle, spleen, stomach and tumour. Impulse response functions (IRFs) corresponding to these tissues were determined by spectral analysis of the tissue TACs [13]. The average IRFs for each common tissue type were obtained by averaging the spectral coefficients across the subjects and convolved with a typical arterial input function, resulting in typical TACs for each tissue. The TACs were then assigned to the corresponding tissue types in a single slice of the Zubal phantom [10] which included blood vessels, bone, liver, bone marrow, muscle, spleen, stomach, and a large and small tumour in the liver (see Figure 1). A dynamic sequence of sinograms was obtained by forward projecting the images into 3.13 mm bins on a  $192 \times 256$  grid. Poisson noise and blurring were also added to simulate realistic sinograms acquired on an ECAT 951R scanner. Noisy dynamic images were then reconstructed using FBP (Hann filter cut-off at the Nyquist frequency). Figure 2 shows the metabolite-corrected arterial blood curve and noisy 2- $^{11}\text{C}$ thymidine kinetics in some representative tissues.

## C. Human Study

The clustering algorithm has been applied to a range of FDG-PET studies and we illustrate its use with a dynamic lung study. The dynamic lung FDG-PET study was performed on a male patient with an aggressive pleural tumour in the left lung. Ethical permission was obtained from our Institutional Review Board. The PET study was commenced after intravenous injection

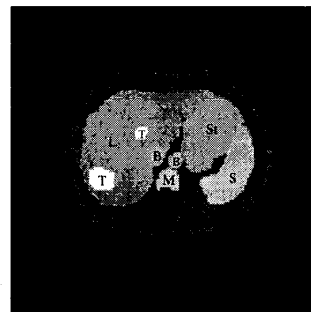


Figure 1: A slice of the Zubal phantom. B = blood vessels; b = bone; L = liver; M = marrow; Mu = muscle; S = spleen; St = stomach; T = tumour.

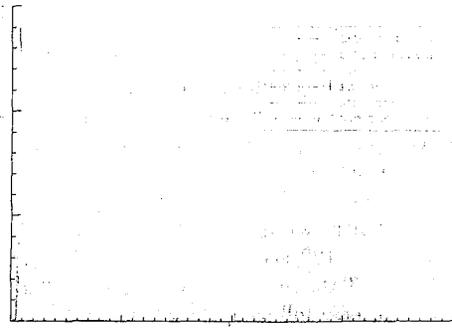


Figure 2: Simulated noisy 2-[<sup>11</sup>C]thymidine kinetics in some representative regions. A metabolite-corrected arterial blood curve which was used to simulate 2-[<sup>11</sup>C]thymidine kinetics in different tissues is also shown.

of 487 MBq of FDG. Emission data were acquired on a ECAT 951R whole-body PET tomograph (CTI/Siemens, Knoxville, TN) over 60 min (22 frames, 6 × 10 sec, 4 × 30 sec, 1 × 2 min, and 11 × 5 min). Twenty-one arterial blood samples were taken from the pulmonary artery to form an input function for kinetic modelling. Separate foci of increased FDG uptake are seen on the right side of the midline in lymph nodes despite the increased uptake at the tumour in the left lung near the chest wall.

### III. RESULTS

#### A. Phantom Study

Figure 3 shows the segmentation results using different numbers of clusters,  $k$ , in the clustering algorithm. The number of clusters is actually varied from 3 to 13 but only some representative samples are shown. In each of the images in Figure 3(a)–(f), different grey levels are used to represent the cluster locations. Figure 3 shows that when the number of clusters is small, segmentation of the data is poor. With  $k = 3$ , the liver, marrow and spleen merge to form a cluster and the other regions merge to form a single cluster. With  $5 \leq k \leq 7$ , the segmentation results improve because the blood vessels and stomach are visualised. However, the hepatic tumours are not seen and the liver and spleen are classified into the same cluster. With  $k = 8$ , the tumours are visualised and almost all of the regions are correctly identified [Figure 3(d)]. Increasing the value of  $k$  to 9 gives nearly the same segmentation as in the case of  $k = 8$  [Figure 3(e)]. Further increasing the value of  $k$ , however, may result in poor segmentation because the actual number of tissues present in the data is less than the specified number of clusters. Homogeneous regions are therefore defragmented to satisfy the constraint on the number of clusters [Figure 3(f)]. Thus, 8 or 9 clusters appear to provide reasonable segmentation of tissues in the slice and this number agrees with the various tissues present in the data.

Figure 4 plots the average mean squared error (MSE)

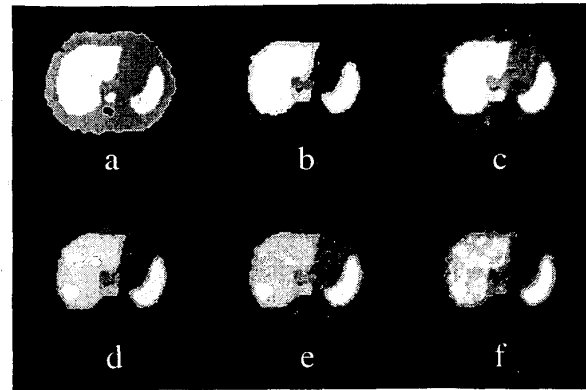


Figure 3: Tissue segmentation obtained with different number of clusters. (a)  $k = 3$ , (b)  $k = 5$ , (c)  $k = 7$ , (d)  $k = 8$ , (e)  $k = 9$ , (f)  $k = 13$ .

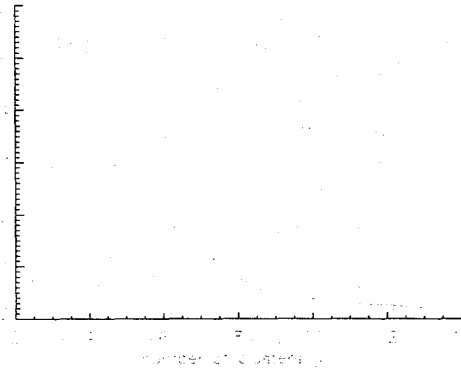


Figure 4: Average mean squared error as a function of number of clusters.

across clusters as a function of  $k$ . The average MSE decreases monotonically, as it drops rapidly ( $k < 8$ ), then decreases less rapidly ( $8 \leq k \leq 9$ ) before reaching a plateau ( $k \geq 10$ ). From the trend of the plot, there is no significant reduction in the average MSE with  $k > 12$ . Furthermore, the decrease in the average MSE is nearly saturated with  $k \geq 8$ . These results confirm the findings of the images in Figure 3, suggesting 8 or 9 as the optimal number of clusters for this dataset.

Application of the clustering algorithm to the simulated PET data is shown in Figure 5. The assumed number of clusters is eight. The signal-to-noise ratio of the images is markedly improved after clustering. In addition, the blood vessels are clearly seen in the frame sampled at 75 sec after clustering but not in the corresponding frame in the original data. In the original images, it is difficult to identify different tissues which may be due to reconstruction effects and inhomogeneous noise. However, the liver, spleen, muscle, marrow, stomach and tumours, are clearly delineated by the clustering algorithm (bottom row of the figure).

#### B. Human Study

Cluster analysis was applied to the dynamic lung FDG-PET data and the results are shown in Figure 6. As there is no *a priori* knowledge about the optimum

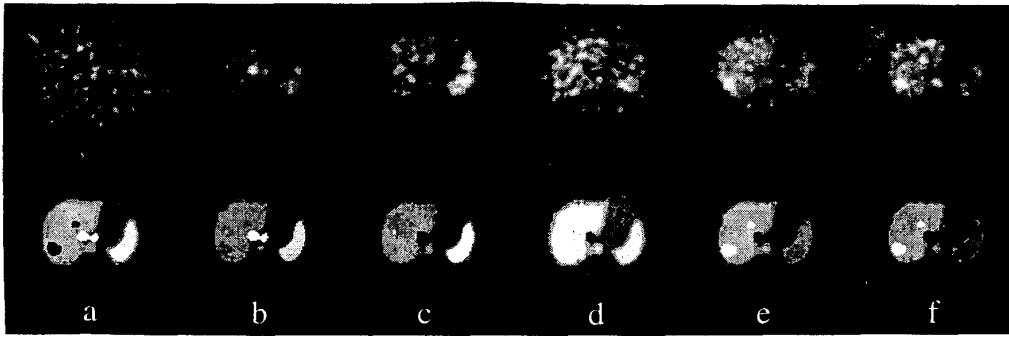


Figure 5: Some selected frames of the simulated 2-[<sup>11</sup>C]thymidine PET study. The top row shows the original reconstructed images, and the bottom row shows the same frames after cluster analysis. Image frames were taken at (a) 15 sec, (b) 75 sec, (c) 135 sec, (d) 285 sec, (e) 1020 sec, and (f) 2850 sec postinjection. Individual images were scaled to their own maximum.

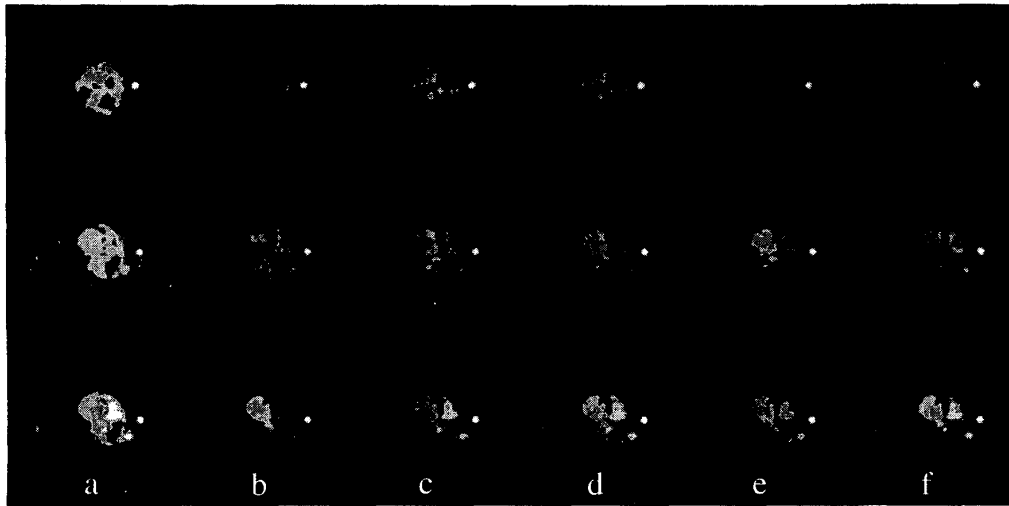


Figure 6: Tissue segmentation of the dynamic lung FDG-PET data in three selected slices - 4 (top row), 19 (middle row) and 24 (bottom row) with different number of clusters: (a)  $k = 4$ , (b)  $k = 7$ , (c)  $k = 8$ , (d)  $k = 9$ , (e)  $k = 10$ , (f)  $k = 12$ .

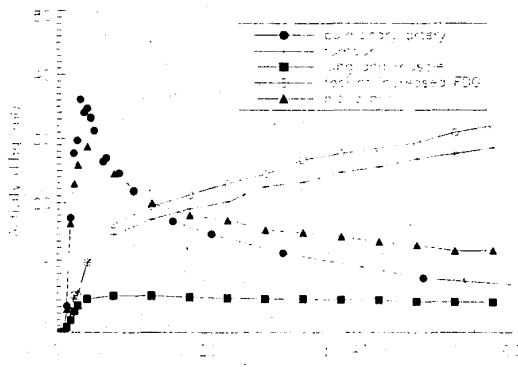


Figure 7: Extracted tissue TACs corresponding to the tumour, lung and muscle, foci of increased FDG uptake, and the blood pool. The measured blood TAC at the pulmonary artery is also shown.

number of clusters in practice, the number of clusters was varied from 3 to 15 so that the possible optimum segmentation of the data set is covered. Only some representative segmentations for the selected slices are

present in the figure.

The optimum numbers of clusters for the selected slices (4, 19, and 24) were found to be 8, 8, and 9, respectively. This is not surprising that the optimum number of clusters is differed for different slices because of the differed number of underlying anatomical structures and the variability of FDG accumulation in a given tissue. Nevertheless, the tumour (slice 4), right lung and muscle (slices 4, 19 and 24), blood pool (slices 4, 19 and 24), separate foci of increased FDG uptake (slices 19 and 24), and the injection site (slices 4, 19 and 24) can be identified with the optimum number of clusters, as seen from the figure. Figure 7 shows the measured blood TAC at the pulmonary artery and the extracted tissue TACs for the tumour (from slice 4), lung and muscle (from slice 19), foci of increased FDG uptake (from slice 24), and the blood pool (from slice 19) using the corresponding optimal value of clusters.

#### IV. DISCUSSION

We have described a tissue segmentation scheme for dynamic PET data using cluster analysis. The proposed

scheme is an attempt to overcome some of the limitations associated with the conventional ROI analysis. It is able to provide statistically meaningful clusters because the entire sequence of images are analysed and different regions whose associated kinetics differed are extracted from the data. Once the segmentation process is finished, the extracted TACs, i.e. the cluster centroids, are then mapped back onto the original data space for all voxels. Thus, an improved signal-to-noise ratio can be achieved because each voxel in the mapped data space is represented by one of the cluster centroids each of which possesses a higher statistical significance than an individual TAC in the same spatial location as it is derived from many TACs of similar kinetic behaviour in the original data space. Therefore, the extracted TACs by cluster analysis may be more consistent and reproducible than those obtained by manual ROI delineation which has inter- and intra-raters variability.

We limited the range for the values of  $k$  and applied the clustering algorithm to the simulated data. Nevertheless, it is reasonable to assume that the limited number of clusters used in this study is feasible, given that there is a finite number of kinetics present in the data. It is, however, desirable to have objective criteria to determine the range that covers possible values of  $k$  or the optimum value of  $k$  that yields optimum segmentation. We are currently exploring various approaches to this problem.

Our clustering algorithm may be useful as a pre-processing step before fast generation of parametric images since only a few characteristic curves need be fitted as compared to conventional pixel-by-pixel parametric image generation where many thousands of tissue TAC must be analysed. The computational advantage and time savings are apparent. In addition, the storage space required for the whole sequence of dynamic images is markedly reduced since only  $k$  characteristic curves and the locations of the clusters need be stored. This greatly facilitates data retrieval and data transmission via the intranet/internet.

## V. CONCLUSIONS

We present an approach to automatically segment tissues in dynamic PET images using cluster analysis. Our preliminary data indicate that accurate tissue segmentation can be achieved and may replace manual ROI delineation. This approach may be potentially useful as a pre-processing step before fast generation of parametric images since computational intensive pixel-by-pixel curve fitting is avoided. Our results have encouraged us to investigate the applicability of this approach to whole-body PET for lesion localisation and assessment of treatment response in a variety of oncological conditions.

## VI. ACKNOWLEDGEMENTS

This work was supported by the National Health and Medical Research Council (NHMRC) of Australia under Grant No. 980042.

## VII. REFERENCES

- [1] H. E. Cline, W. E. Lorensen, R. Kikinis, and F. A. Jolesz, "Three-dimensional segmentation of MR images of the head using probability and connectivity," *J. Comput. Assist. Tomogr.*, vol. 14, pp. 1037-1045, 1990.
- [2] Z. Liang, J. R. MacFall, and D. P. Harrington, "Parameter estimation and tissue segmentation from multispectral MR images," *IEEE Trans. Med. Imag.*, vol. 13, pp. 441-449, 1994.
- [3] W. M. Wells, III, W. E. L. Grimson, R. Kikinis, and F. A. Jolesz, "Adaptive segmentation of MRI data," *IEEE Trans. Med. Imag.*, vol. 15, pp. 429-442, 1996.
- [4] I. Jolliffe, *Principal Component Analysis*, Springer, New York, USA, 1986.
- [5] F. Pedersen, M. Bergström, and B. Långström, "Principal component analysis of dynamic positron emission tomography images," *Eur. J. Nucl. Med.*, vol. 21, pp. 1285-1292, 1994.
- [6] H. M. Wu, C. K. Hoh, D. B. Buxton, H. R. Schelbert, Y. Choi, R. A. Hawkins, M. E. Phelps, and S. C. Huang, "Factor analysis for extraction of blood time-activity curves in dynamic FDG-PET studies," *J. Nucl. Med.*, vol. 36, pp. 1714-1722, 1995.
- [7] M. C. Gregoire, F. Frouin, F. Lavenne, O. de Dreuille, M. Janier, R. Di Paola, and L. Cinotti, "Evaluation of factor analysis accuracy for myocardial perfusion in PET studies," *Conf. Record, 1995 IEEE Medical Imaging Conf.*, pp. 1689-1693, 1995.
- [8] J. A. Hartigan, *Clustering Algorithms*, Wiley, New York, U.S.A., 1975.
- [9] J. Ashburner, J. Haslam, C. Taylor, V. J. Cunningham, and T. Jones, "A cluster analysis approach for the characterization of dynamic PET data," in *Quantification of Brain Function using PET*, R. Myers, V. Cunningham, D. Bailey, and T. Jones, Eds., pp. 301-306. Academic Press, San Diego, 1996.
- [10] I. G. Zubal, C. R. Harrell, E. O. Smith, Z. Rattner, G. Gindi, and P. B. Hoffer, "Computerized three-dimensional segmented human anatomy," *Med. Phys.*, vol. 21, pp. 299-302, 1994.
- [11] L. Cooper, "M-dimensional location models: Application to cluster analysis," *J. Reg. Sci.*, vol. 13, pp. 41-54, 1973.
- [12] S. R. Meikle, J. C. Matthews, V. J. Cunningham, D. L. Bailey, L. Livieratos, T. Jones, and P. Price, "Parametric image reconstruction using spectral analysis of PET projection data," *Phys. Med. Biol.*, vol. 43, pp. 651-666, 1998.
- [13] V. J. Cunningham and T. Jones, "Spectral analysis of dynamic PET studies," *J. Cereb. Blood Flow Metab.*, vol. 13, pp. 15-23, 1993.